Preparation of $(La_{0.8}Sr_{0.2})_2FeNiO_{6-\delta}$ Nanopowder by Pechini Method and Its Sensitivity to NO_2

Lihong Zhou[1], Wei Duan[1], Bikang Hu[1] and Jianzhong Xiao[2,a]

[1]City College, Wuhan University of Science and Technology, Wuhan, Hubei 430083, P. R. China
[2]State Key Laboratory of Materials Processing and Die & Mold Technology, School of Materials Science and Engineering, Huazhong University of Science and Technology, Wuhan, Hubei 430074, P. R. China

Abstract. The nano-sized $(La_{0.8}Sr_{0.2})_2FeNiO_{6-\delta}$ (LSFN) double perovskite powder without impurity phase was successfully prepared using the Pechini method. The result demonstrated that the electrode sensing properties to NO_2 were affected by the sintering temperature. The sensor with 1300 ℃ -sintered LSFN sensing electrode exhibited the highest NO_2 sensitivity.

1 Introduction

The increasing amount of NO_2 emissions from automobiles and various industrial processes has caused serious environmental pollution such as photochemical smog and acid rain[1]. In-vehicle NO_2 sensors are required to monitor and determine the regeneration time of the NO_2 reduction catalyst in the next-generation lean-burn gasoline or diesel engine in an integrated on-board diagnostic system for exhaust gas monitoring and feedback control[2]. Since the sensors installed in the exhaust gas post-processing system must be able to withstand the harsh conditions of high temperature, high humidity, and coexistence of multiple gases, a high-temperature NO_2 gas sensor with excellent sensing performance is required. Among the many gas sensors, solid-state sensors based on yttria-stabilized zirconia (YSZ) electrolytes and metal oxide sensing electrodes (SE) have become the most promising devices due to their low cost, compactness, sensitivity, and reliability. And it is getting more and more attention from researchers or teams all over the world[2].

So far, some high temperature potential[3-5], impedance[6-7] and current [8-9]YSZ based gas sensors have been developed for the detection of NO_2. Among them, mixed potential type gas sensors using YSZ as an electrolyte have been extensively studied. For mixed-potential sensors, the development of suitable sensing electrode materials plays an important role in improving the sensing performance of NO_2. A lot of work has been done to explore high-performance sensing electrode materials ranging from single metal oxides to complex perovskites and spinel oxides[10-14]. Recently, double perovskite electrode materials have attracted attention due to their higher conductivity and catalytic activity. The $(La_{0.8}Sr_{0.2})_2FeNiO_{6-\delta}$ (LSFN) is a potential candidate for SEs of NOx sensors[15]. Zhuiykov et al.[16] found that adding 0.01wt.% Pt to sensitive electrode of $ZnFe_2O_4$ can reduce the response time about 5min of 436 ppm NO_2 at 700 °C compared with $ZnFe_2O_4$-SE. The improvement of the sensing characteristics was possible by a small amount of a noble metal Pt. Zhou et al.[15] used Pt paste for sensitivity testing of LSFN. In order to more realistically test the sensitivity of NO_2 to LSFN-SE, this test uses Ag as an electrical connection and Ag paste as a current collector to test the sensitivity of sensitive electrodes to NO_2. In addition to the nature of the sensitive electrode material itself, the preparation method has a greater impact on the NO_2 sensitivity of the material. Powders prepared by different methods have large differences in surface properties and structures. Among them, the powder obtained by sol-gel method and combustion method has high catalytic activity, large specific surface area, and uniform particle size, and thus has been widely studied and applied. Herein, we used the Pechini method in the sol-gel method to prepare nano-sized LSFN powder.

2 Experimental

2.1 Powder synthesis

La_2O_3, $Sr(NO_3)_2$, $Fe(NO_3)_3 \cdot 9H_2O$, and $Ni(NO_3)_2 \cdot 6H_2O$ are used as raw materials. The oxides and nitrates are weighed in an elemental molar ratio of La:Sr:Fe:Ni=1.6:0.4:1:1. La_2O_3 was dissolved with dilute HNO_3, each nitrate was dissolved with deionized water, and they were mixed together. The citric acid (CA) and ethylene glycol (EG) were used as monomers for forming the poly-meric matrix. The molar ratio of CA to EG is 1:4. The resulting mixture was heated and stirred in a constant temperature water bath at 80 °C to evaporate. Finally, a dark green transparent polymeric resin precursor was obtained. After it was sufficiently dried at 130 °C, it swelled to form an internally porous, complete three-dimensional polymer framework. Then the carbonaceous components were combusted by

* Corresponding author: jzxiao@mail.hust.edu.cn

precalcining the dried gel at 400°C for 10 h. Finally, grind the obtained powder for 30 min and calcine it at 800 °C in air for 10 h to yield the LSFN powder.

2.2 Sensor fabrication

The sensor is composed of YSZ, SE and reference electrode (RE), the structure of which is shown in Figure 1. The YSZ disc (5 mol% Y_2O_3-doped ZrO_2, Ø16 mm × 0.5 mm) was fabricated by sintering at 1450 °C for 2.5 h in air. The LSFN powder and an organic binder (α-terpineol and ethyl cellulose) were mixed thoroughly to a weight ratio of 2:3. The resulting paste was printed on one side of YSZ disc to form the LSFN–SE(Ø11.3 mm), and then they were dried at 80 °C for 2 h after being kept at room temperature for 12 h in atmospheric air and subsequently sintered at 1100, 1200 and 1300 °C for 1 h, also in air. The Pt reference electrode (Ø11.3 mm) was screen printed using the commercial Pt paste on the other side of the YSZ disc and then sintered at 1000 °C for 2 h in air.

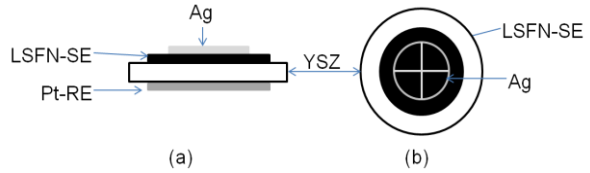

Figure 1. The schematic of the NO_2 sensor (a) side view, (b) top view.

2.3 Characterization

A thermal analyzer (TG/DTA) (Diamond TG/DTA, PerkinElmer Instruments) was used to measure the mass changes and thermal behaviors of the gel from room temperature to 800 °C, and the heating rate was 10 °C/min in air atmosphere. The crystal structure of the LSFN powder and LSFN-SEs were examined by XRD (X′Pert PRO, PANalytical B. V., Holland) with Cu-kα radiation. The calcined powder was observed using a JSM-7600F field emission scanning electron microscope manufactured by JEOL. Surface morphology of LSFN-SEs was observed by ESEM (Quanta 200, FEI, Holland) operating at 20 kV.

2.4 Testing parameters

Sensor experiments were conducted in a gas-flow apparatus (MPA-80). Gas environments were controlled using mass flow controllers (Beijing Seven Star Electronics Company). The total flow rate was set at a constant 200 ml min^{-1}. The fabricated sensors were exposed to base gas with 10 % O_2 balanced by N_2. NO_2 was exposed to the sensors in the following concentrations : 100, 200, 400, 600 and 800 ppm. The test temperature was kept at 550 °C. The Pt wires were respectively soldered to the surfaces of SE and RE with Ag paste to collect electrical signals. At the same time, the surface of the SE was brushed with Ag paste to form the pattern shown in Fig. 1 for current collection. The voltage between the SE and RE was measured during the step changes using an electrochemical workstation (VearsaSTAT3, Princeton, USA). Both electrodes of the sensor were in the same gas atmosphere.

3 Results and discussion

3.1 Powder characterization

Fig. 2 is a TG-DTA curve of a gel with CA/M=0.8, pH=9. An endothermic peak at 139.7 °C may be caused by the decomposition of the structural water. At 225-250 °C, the weight loss was about 45 %, and the weight loss curve decreased vertically. Accompanying the exothermic peak at 231.8 °C, the organic matter and nitrates exploded and decomposed. The weight loss curve did not change substantially above 350 °C.

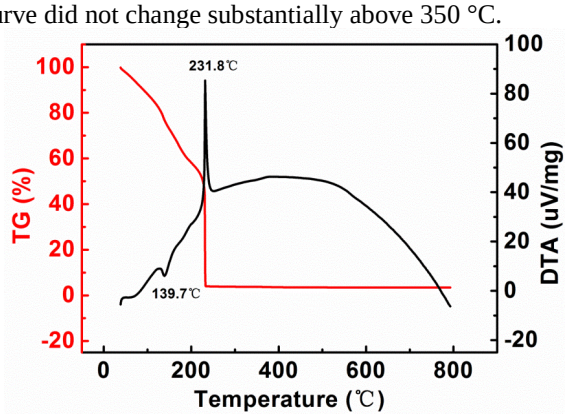

Figure 2. TG-DTA curve of dried LSFN gel.

Fig. 3 shows the XRD patterns of LSFN powder sintered at 800 °C and the LSFN-SE on YSZ substrates sintered at different temperatures from 1100 to 1300 °C. The XRD data shows no impurities exist in the synthesized powder and all there flections were characteristic of a cubic double perovskite LSFN phase (space group Pm-3m, JCPDS No.74-1975). As shown in Fig. 4, the strongest peak of the SE sintered at 1100 °C splits into two peaks. With the increase of the sintering temperature, the strongest peak gradually shifts to the left. The cubic to rhombohedra phase transformation occurs for the SE sintered at 1100 °C, and the other two sintering temperature samples are still cubic phase. However, the cell parameters increase slightly, from a=b=c=3.8741 Å of LSFN powder to a=b=c=3.8900 Å of the SE sintered at 1300 °C. This indicates that the LSFN structure is affected by the sintering temperature. At the same time, the diffraction peaks of YSZ can also be observed in the LSFN-SEs. The main crystal phase ZrO_2 in YSZ is also cubic symmetrical structure.

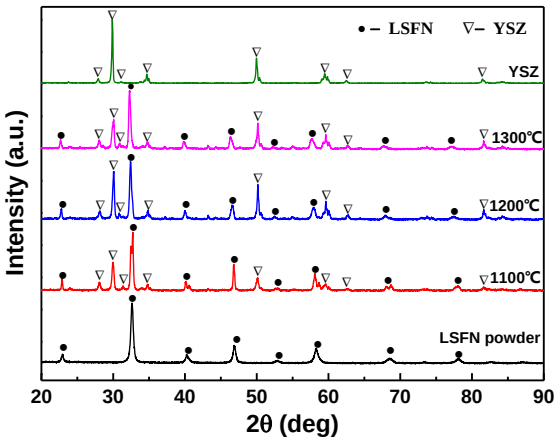

Figure 3. The XRD patterns of the LSFN powder and the LSFN sensing electrodes sintered at different temperatures on YSZ substrates.

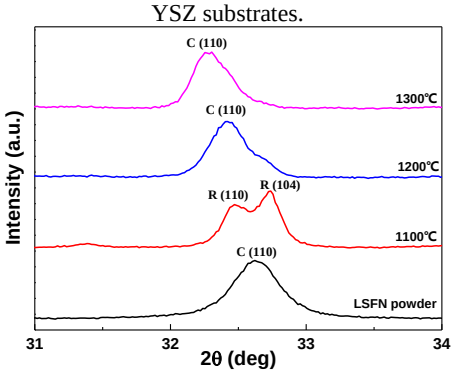

Figure 4. The enlarge drawing of the corresponding strongest peaks from Fig. 3.

Fig. 5 shows the FSEM topography of the LSFN powder calcined at 800 °C. The particle size of the powder is uniform, the average particle size is about 80-90 nm, but there is agglomeration phenomenon. This demonstrates the successful preparation of nano-sized powders using the Pechini method.

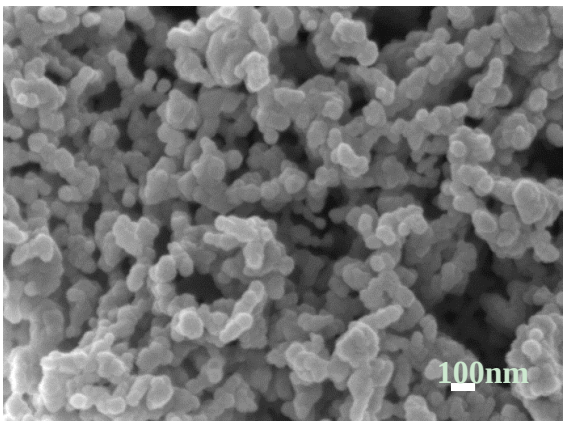

Figure 5. FSEM morphology of LSFN powder calcined at 800 °C.

As can be seen from Fig. 6, as the sintering temperature increases, LSFN particles gradually grow. The corresponding average sizes were 0.12 (120 nm), 1.2, and 1.5 μm, respectively. When the sintering temperature reaches 1200 °C, the grain growth is particularly noticeable. Above 1200 °C, there is a significant sintering phenomenon between the LSFN particles, and sintered necks are formed between the particles. With the increase of sintering temperature, the size of particles and pores becomes larger, the film thickness decreases (which are respectively 14.8, 7.4 and 5.2 μm), and the electrode and YSZ bond more and more firmly.

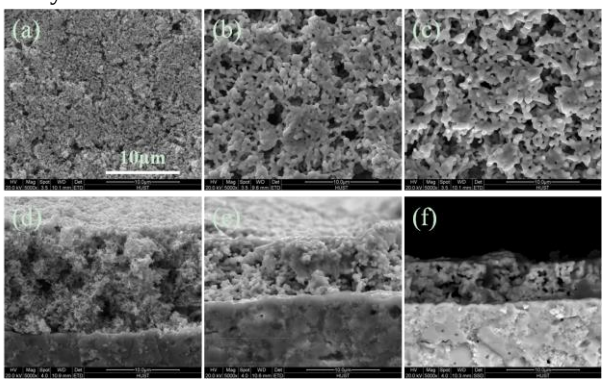

Figure 6. The surface morphology of LSFN-SEs sintered at different temperatures (a) 1100°C, (b) 1200°C and (c) 1300°C and cross-sectional views (d) 1100°C (e) 1200°C (f) 1300°C.

3.2 Sensing properties

Fig. 7 shows the response/recovery transients to the different NO_2 concentrations at 550 °C for the sensors with each LSFN-SE sintered at different temperature and the corresponding dependence of ΔV on NO_2 concentrations. The ΔV (V_{sample}− $V_{base\ gas}$) values of the sensors were almost linear to the logarithm of NO_2 concentrations examined. As the sintering temperature increases, the slope increases sequentially. The slopes for 1100 °C and 1200 °C are very close, but for 1300 °C increases dramatically. The corresponding slopes are 38.38, 59.24, and 130.17mV/decade, respectively.

The sensor of LSFN-SE sintered at 1300 °C has the highest sensitivity to NO_2. It is clear that the sintering temperature affects the sensitivity of the SE to NO_2. As we all know, the finer the electrode particles, the higher the catalytic activity, i.e., the lower sintering temperature has better NO_2 sensitivity, but the test results are contrary to the theory. According to the literature[17], this may be due to inconsistent gas-phase catalytic decomposition of NO_2 by different SE matrix. Although the LSFN-SE sintered at 1100 °C has fine particles and high catalytic activity, the decomposition rate of NO_2 is the highest. At the same time, its thickness is nearly 3 times that of the SE sintered at 1300 °C, and the long NO_2 diffusion path also leads to more decomposition of NO_2, although the rhombohedra phase of the SE sintered at 1100 °C may have high catalytic activity for NO_2[18]. The combination of the above factors eventually led to a sensor with the LSFN-SE sintered at 1100 °C with a minimum sensitivity to NO_2. From Fig. 7 we also observed that as the sintering temperature increases, the recovery rate decreases.

The sensor with the LSFN-SE sintered at 1100 °C has a response potential of 15.3 mV for 200 ppm NO_2 at 550 °C. However, the corresponding sensor with Pt slurry welding has a higher potential of 53.7 mV, with other test conditions unchanged[15]. Obviously, precious metal Pt on the surface of LSFN-SE for welding greatly

improves the sensitivity of SE to NO_2.

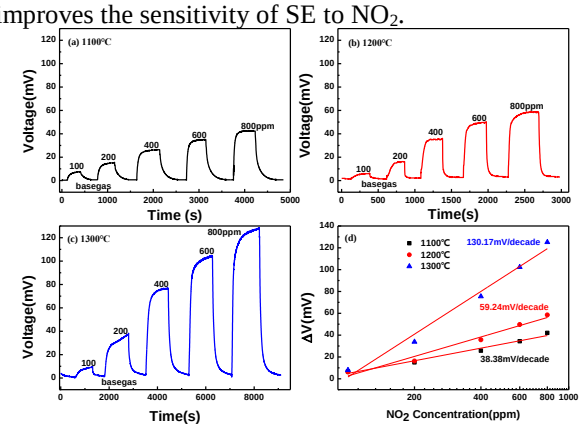

Figure 7. Response/recovery transients to the different NO_2 concentrations at 550 °C for the sensors with each LSFN-SE sintered at different temperatures (a) 1100, (b) 1200 and (c) 1300 °C and the corresponding logarithm of NO_2 concentration versus potential (d).

4 Conclusions

In this paper, an oxide $(La_{0.8}Sr_{0.2})_2FeNO_{6-\delta}$ with a double-perovskite structure, which was used as the sensing electrode of YSZ-based NO_2 sensors, was successfully synthesized. The results demonstrated that the symmetry structure of LSFN sensing electrode was affected by the sintering temperature. The change of sintering temperature also has a large effect on the microstructure and the thickness of SE. These changes would vary the NO_2 sensitivity of the sensors. The highest NO_2 sensitivity was obtained by the sensor with 1300 °C-sintered LSFN sensing electrode, and its sensitivity is up to 130.17 mV/decade.

References

1. R. Moos, B. Reetmeyer, A. Hürland, C. Plog, Sens. Actuators B: Chem. **119(1)** 57-63 (2006)
2. F. Liu, B. Wang, X. Yang, Y. Guan, Q. Wang, X. Liang, P. Sun, Y. Wang, G. Lu, Sens. Actuators B: Chem. **240** 148-157 (2017).
3. S. Zhuiykov, T. Nakano, A. Kunimoto, N. Yamazoe, N. Miura, Electrochem. Commun. 3(**2**) 97-101 (2001)
4. E.R. Macam, B.M. Blackburn, E.D. Wachsman, Sens. Actuators B: Chem. **158(1)** 304-312 (2011)
5. J. Zosel, D. Franke, K. Ahlborn, F. Gerlach, V. Vashook, U. Guth, Solid State Ion. **179(27)** 1628-1631 (2008)
6. L.P. Martin, L.Y. Woo, R.S. Glass, J. Electrochem. Soc. **3** J97-J104 (2007)
7. N. Miura, M. Nakatou, S. Zhuiykov, Sens. Actuators B: Chem. **93(1-3)** 221-228 (2003)
8. J.C. Yang, P.K. Dutta, Sens. Actuators B: Chem. **123(2)** 929-936 (2007)
9. T. Ueda, T. Nagano, H. Okawa, S. Takahashi, Electrochem. Commun. **11(8)** 1654-1656 (2009)
10. G. Lu, N. Miura, N. Yamazoe, Sens. Actuators B: Chem. **65(1-3)** 125-127 (2000)
11. N. Miura, J. Wang, M. Nakatou, P. Elumalai, S. Zhuiykov, M. Hasei, Sens. Actuators B: Chem. **114(2)** 903-909 (2006)
12. E.R. Macam, B.M. Blackburn, E.D. Wachsman, Sens. Actuators B: Chem. **157(2)** 353-360 (2011)
13. N. Miura, S. Zhuiykov, T. Ono, M. Hasei, N. Yamazoe, Sens. Actuators B: Chem. **83(1-3)** 222-229 (2002)
14. J.W. Yoon, M.L. Grilli, E.D. Bartolomeo, R. Polini, E. Traversa, Sens. Actuators B: Chem. **76(1-3)** 483-488 (2001)
15. L. Zhou, X. Li, H. Wu, Z. Liao, Q. Yuan, F. Xia, J. Xiao, Ceram. Int. **40(7)** 9257-9263 (2014)
16. S. Zhuiykov, T. Ono, N. Yamazoe, N. Miura, Solid State Ion. **152(8)** 801-807 (2002)
17. P. Elumalai, J. Wang, S. Zhuiykov, D. Terada, M. Hasei, N. Miura, J. Electrochem. Soc. **152(7)** H95-H101 (2005)
18. L. Zhou, Q. Yuan, X. Li, J. Xu, F. Xia, J. Xiao, Sens. Actuators B: Chem. **206(206)** 311-318 (2015)